Inorganic Chemistry
Article

Inorg. Chem. **2010**, *49*, 2325–2333 **2325**
DOI: 10.1021/ic902231b

Ternary Rare-Earth Iron Arsenides $RE_{12}Fe_{57.5}As_{41}$ (RE = La, Ce)

Stanislav S. Stoyko, Peter E. R. Blanchard, and Arthur Mar*

Department of Chemistry, University of Alberta, Edmonton, Alberta, Canada T6G 2G2

Received November 11, 2009

The rare-earth iron arsenides $RE_{12}Fe_{57.5}As_{41}$ (RE = La, Ce) have been prepared by direct reactions of the elements in the presence of a Sn flux. Analysis of single-crystal X-ray diffraction data reveals that they adopt a new orthorhombic structure type (Pearson symbol *oP*236, space group *Pmmn*, Z = 2; a = 10.8881(9) Å, b = 25.753(2) Å, c = 12.5436(10) Å for RE = La; a = 10.8376(8) Å, b = 25.639(2) Å, c = 12.4701(9) Å for RE = Ce). In this metal-rich arsenide, the complex three-dimensional network (derived from 4 RE, 24 Fe, and 17 As sites) can be described as being built from unusual wavelike layers of connected As-centered trigonal prisms. Five of the Fe sites are partially occupied. The electronic structure of these compounds was probed through core-line X-ray photoelectron spectra. Magnetic susceptibility measurements indicated ferromagnetic ordering at T_C = 125 and 95 K for the La and Ce compounds, respectively. Electrical resistivity measurements on single crystals of $Ce_{12}Fe_{57.5}As_{41}$ showed metallic behavior with a prominent transition that coincides closely with the ferromagnetic ordering temperature.

Introduction

With the recent burst of activity prompted by the discovery of superconductivity in iron-based arsenides and oxyarsenides such as doped $BaFe_2As_2$ and LaFeAsO,[1−5] it is important to establish phase relationships in the parent ternary pnictide systems. Although comprehensive reviews of ternary rare-earth phosphides,[6] antimonides,[7] and even bismuthides are now available,[8] a corresponding one for the arsenides is still absent because of the relative lack of systematization of their structures and properties. In fact, to the best of our knowledge, no phase diagram information is available for any of the ternary RE−Fe−As systems. Reports in these systems have been restricted to several isolated phases: $REFe_4As_{12}$ (RE = La−Nd, Sm),[9−18] $EuFe_2As_2$,[19−26] REFeAs (RE = La−Nd),[20] and $RE_6Fe_{13}As$ (RE = Pr, Nd).[27]

*To whom correspondence should be addressed. E-mail: arthur.mar@ualberta.ca.

(1) Rotter, M.; Tegel, M.; Johrendt, D. *Phys. Rev. Lett.* **2008**, *101*, 107006-1–107006-4.
(2) Rotter, M.; Pangerl, M.; Tegel, M.; Johrendt, D. *Angew. Chem., Int. Ed.* **2008**, *47*, 7949–7952.
(3) Kamihara, Y.; Watanabe, T.; Hirano, M.; Hosono, H. *J. Am. Chem. Soc.* **2008**, *130*, 3296–3297.
(4) Johrendt, D.; Pöttgen, R. *Angew. Chem., Int. Ed.* **2008**, *47*, 4782–4784.
(5) Pöttgen, R.; Johrendt, D. *Z. Naturforsch. B* **2008**, *63*, 1135–1148.
(6) Kuz'ma, Yu.; Chykhrij, S. In *Handbook on the Physics and Chemistry of Rare Earths*; Gschneidner, K. A., Jr., Eyring, L., Eds.; Elsevier: Amsterdam, The Netherlands, 1996; Vol. *23*, pp 285−434.
(7) Sologub, O. L.; Salamakha, P. S. In *Handbook on the Physics and Chemistry of Rare Earths*; Gschneidner, K. A., Jr., Bünzli J.-C. G., Pecharsky, V. K., Eds.; Elsevier: Amsterdam, The Netherlands, 2003; Vol. *33*, pp 35−146.
(8) Mar, A. In *Handbook on the Physics and Chemistry of Rare Earths*; Gschneidner, K. A., Jr., Bünzli J.-C. G., Pecharsky, V. K., Eds.; Elsevier: Amsterdam, The Netherlands, 2006; Vol. *36*, pp 1−82.
(9) Braun, D. J.; Jeitschko, W. *J. Solid State Chem.* **1980**, *32*, 357–363.
(10) Grandjean, F.; Gérard, A.; Braun, D. J.; Jeitschko, W. *J. Phys. Chem. Solids* **1984**, *45*, 877–886.
(11) Jeitschko, W.; Foecker, A. J.; Paschke, D.; Dewalsky, M. V.; Evers, Ch. B. H.; Künnen, B.; Lang, A.; Kotzyba, G.; Rodewald, U. Ch.; Möller, M. H. *Z. Anorg. Allg. Chem.* **2000**, *626*, 1112–1120.
(12) Shirotani, I.; Ohno, K.; Sekine, C.; Yagi, T.; Kawakami, T.; Nakanishi, T.; Takahashi, H.; Tang, J.; Matsushita, A.; Matsumoto, T. *Physica B* **2000**, *281*−*282*, 1021–1023.
(13) Watcharapasorn, A.; Feigelson, R. S.; Caillat, T.; Borshchevsky, A.; Snyder, G. J.; Fleurial, J.-P. *J. Appl. Phys.* **2002**, *91*, 1344–1348.
(14) Harima, H.; Takegahara, K. *Physica B* **2003**, *328*, 26–28.
(15) Sayles, T. A.; Yuhasz, W. M.; Paglione, J.; Yanagisawa, T.; Jeffries, J. R.; Maple, M. B.; Henkie, Z.; Pietraszko, A.; Cichorek, T.; Wawryk, R.; Nemoto, C.; Goto, T. *Physica B* **2008**, *403*, 869–870.
(16) Kikuchi, D.; Tatsuoka, S.; Tanaka, K.; Kawahito, Y.; Ueda, M.; Shinozawa, A.; Aoki, H.; Kuwahara, K.; Aoki, Y.; Sato, H. *Physica B* **2008**, *403*, 884–886.
(17) Tatsuoka, S.; Sato, H.; Tanaka, K.; Ueda, M.; Kikuchi, D.; Aoki, H.; Ikeno, T.; Kuwahara, K.; Aoki, Y.; Sugawara, H.; Harima, H. *J. Phys. Soc. Jpn.* **2008**, *77*, 033701-1–033701-4.
(18) Sayles, T. A.; Yuhasz, W. M.; Paglione, J.; Yanagisawa, T.; Jeffries, J. R.; Maple, M. B.; Henkie, Z.; Pietraszko, A.; Cichorek, T.; Wawryk, R.; Nemoto, C.; Goto, T. *Phys. Rev. B* **2008**, *77*, 144332-1–144332-12.
(19) Marchand, R.; Jeitschko, W. *J. Solid State Chem.* **1978**, *24*, 351–357.
(20) Raffius, H.; Mörsen, E.; Mosel, B. D.; Müller-Warmuth, W.; Jeitschko, W.; Terbüchte, L.; Vomhof, T. *J. Phys. Chem. Solids* **1993**, *54*, 135–144.
(21) Tegel, M.; Rotter, M.; Weiss, V.; Schappacher, F. M.; Pöttgen, R.; Johrendt, D. *J. Phys.: Condens. Matter* **2008**, *20*, 452201-1–452201-5.
(22) Ren, Z.; Zhu, Z.; Jiang, S.; Xu, X.; Tao, Q.; Wang, C.; Feng, C.; Cao, G.; Xu, Z. *Phys. Rev. B* **2008**, *78*, 052501-1–052501-4.
(23) Jeevan, H. S.; Hossain, Z.; Kasinathan, D.; Rosner, H.; Geibel, C.; Gegenwart, P. *Phys. Rev. B* **2008**, *78*, 052501-1–052501-4.
(24) Kasinathan, D.; Ormeci, A.; Koch, K.; Burkhardt, U.; Schnelle, W.; Leithe-Jasper, A.; Rosner, H. *New J. Phys.* **2009**, *11*, 025023-1–025023-27.
(25) Ren, Z.; Lin, X.; Tao, Q.; Jiang, S.; Zhu, Z.; Wang, C.; Cao, G.; Xu, Z. *Phys. Rev. B* **2009**, *79*, 094426-1–094426-5.
(26) Wu, D.; Barišić, N.; Drichko, N.; Kaiser, S.; Faridian, A.; Dressel, M.; Jiang, S.; Ren, Z.; Li, L. J.; Cao, G. H.; Xu, Z. A.; Jeevan, H. S.; Gegenwart, P. *Phys. Rev. B* **2009**, *79*, 155103-1–155103-10.
(27) Weitzer, F.; Leithe-Jasper, A.; Rogl, P.; Hiebl, K.; Noël, H.; Wiesinger, G.; Steiner, W. *J. Solid State Chem.* **1993**, *104*, 368–376.

© 2010 American Chemical Society
Published on Web 02/03/2010

Table 1. Crystallographic Data for $RE_{12}Fe_{57.5}As_{41}$ (RE = La, Ce)

formula	$La_{12}Fe_{57.5}As_{41}$	$Ce_{12}Fe_{57.5}As_{41}$
formula mass (amu)	7950.02	7964.54
space group	*Pmmn* (No. 59)	*Pmmn* (No. 59)
a (Å)	10.8881(9)	10.8376(8)
b (Å)	25.753(2)	25.639(2)
c (Å)	12.5436(10)	12.4701(9)
V (Å^3)	3517.2(5)	3465.0(4)
Z	2	2
ρ_{calcd} (g cm^{-3})	7.507	7.634
cryst dimens (mm)	0.07 × 0.07 × 0.38	0.02 × 0.04 × 0.53
radiation	graphite-monochromated Mo Kα, λ = 0.710 73 Å	
μ(Mo Kα) (mm^{-1})	37.67	38.72
transmission factors	0.013−0.147	0.029−0.494
2θ limits	$3.62° \le 2\theta$ (Mo Kα) $\le 66.34°$	$3.64° \le 2\theta$ (Mo Kα) $\le 66.40°$
data collected	$-16 \le h \le 16$, $-39 \le k \le 39$, $-19 \le l \le 19$	$-16 \le h \le 16$, $-38 \le k \le 38$, $-18 \le l \le 18$
no. of data collected	80 029	63 149
no. of unique data, including $F_o^2 < 0$	7090 (R_{int} = 0.190)	6865 (R_{int} = 0.161)
no. of unique data, with $F_o^2 > 2\sigma(F_o^2)$	4920	5340
no. of variables	294	293
$R(F)$ for $F_o^2 > 2\sigma(F_o^2)$[a]	0.041	0.042
$R_w(F_o^2)$[b]	0.094	0.111
GOF	0.970	1.030
$(\Delta\rho)_{max}$, $(\Delta\rho)_{min}$ (e Å^{-3})	5.32, −4.31	5.37, −5.14

[a] $R(F) = \sum||F_o| - |F_c||/\sum|F_o|$. [b] $R_w(F_o^2) = [\sum[w(F_o^2 - F_c^2)^2]/\sum wF_o^4]^{1/2}$; $w^{-1} = [\sigma^2(F_o^2) + (Ap)^2 + Bp]$, where $p = [\max(F_o^2,0) + 2F_c^2]/3$.

All of these compounds are of interest because of their magnetic properties; in addition, $EuFe_2As_2$, if appropriately doped, is a possible candidate for superconductivity given its resemblance to AFe_2As_2 (A = Ca, Ba, Sr).[22−25]

In the course of evaluating the phase equilibria in these RE−Fe−As systems, we have discovered the new phase $RE_{12}Fe_{57.5}As_{41}$, which forms for RE = La and Ce. We report here the syntheses of these compounds, their rather complex crystal structures, their electrical and magnetic properties, and their electronic structures, as evaluated through X-ray photoelectron spectroscopy (XPS).

Experimental Section

Synthesis. The title compounds were first identified as major products from direct reactions of the elements in the presence of a Sn flux. A 0.3 g mixture of RE pieces (La or Ce, 99.9%, Hefa), Fe powder (99.9%, Cerac), and As lumps (99.999%, Alfa-Aesar) in a molar ratio of 1:5:3 was placed in an evacuated fused-silica tube together with a 6-fold (by weight) excess of Sn (99.8%, Cerac). The reaction mixture was stepwise heated to 900 °C over 3 days, held at this temperature for 4 days, and slowly cooled (4 °C/h) to 600 °C, followed by furnace cooling to room temperature. Black needle-shaped crystals of the ternary arsenides $RE_{12}Fe_{57.5}As_{41}$, together with crystals of binary-phase byproduct FeAs, were recovered by dissolving excess Sn flux in diluted HCl. Visual examination revealed that the silica tubes were intact and suffered no deleterious reactions with, for example, the rare-earth metals. Energy-dispersive X-ray (EDX) analysis on these crystals with a Hitachi S-2700 scanning electron microscope gave approximate chemical compositions [12(2)% RE, 50(2)% Fe, and 38(2)% As] that were in good agreement with the formulas ultimately refined from the structure determinations (11% RE, 52% Fe, and 37% As). No other elements heavier than Na (such as Si or Sn) were detected in numerous crystals analyzed. Single-phase polycrystalline samples for magnetic property measurements were prepared by sintering stoichiometric mixtures of the elements at 900 °C for 1 week with intermediate grindings and further annealing at 800 °C for another 1 week. The sample purity was ascertained by analysis of powder X-ray diffraction patterns, collected on an Inel powder diffractometer equipped with a CPS 120 detector. Attempts to prepare other light rare-earth analogues under the same conditions were unsuccessful.

Structure Determination. Single-crystal X-ray diffraction data for $RE_{12}Fe_{57.5}As_{41}$ (RE = La, Ce) were collected on a Bruker Platform/SMART 1000 CCD diffractometer at 22 °C using ω scans. Structure solution and refinement were carried out using the *WinGX* program package.[28] Face-indexed numerical absorption corrections were applied. Crystal data and further details of the data collection are given in Table 1. The intensity pattern and systematic absences were consistent with the orthorhombic space groups *Pmmn* and $Pmn2_1$. Intensity statistics (mean $|E^2 - 1|$ = 0.938 and 0.961 for RE = La and Ce, respectively) favored the centrosymmetric space group *Pmmn*. The initial atomic positions for RE, As, and most of the Fe atoms were found by direct methods. The Fe17 and Fe19 sites exhibited elevated displacement parameters, suggesting partial occupancy. Two additional prominent peaks remaining in the difference electron density map were assigned as partially occupied Fe10 and Fe20 sites. When allowed to refine freely, the occupancies of these sites converged to values [RE = La: 0.55(4) for Fe 17, 0.48(2) for Fe19, 0.22(2) for Fe10, 0.52(2) for Fe20; RE = Ce: 0.50(4) for Fe17, 0.48(1) for Fe19, 0.23(2) for Fe10, 0.52(1) for Fe20] that are close to either 0.50 or 0.25. The occupancies of these sites (Fe17/Fe10 and Fe19/Fe20) are correlated because of chemically impossible short distances between them and symmetry-equivalent positions and are limited to a maximum of 0.50 (for Fe 17, Fe19, and Fe20) or 0.25 (for Fe10). All other sites were essentially fully occupied, except for Fe12, whose occupancy converged to 0.27(1) (for RE = La) or 0.26(1) (for RE = Ce). In the final cycles of refinement, the occupancies of these partially occupied sites were fixed to their idealized values of 0.50 (for Fe17, Fe19, and Fe20) or 0.25 (for Fe10 and Fe12). The formula corresponding to this final structural model is $RE_{12}Fe_{57.5}As_{41}$.

Atomic positions were standardized with the program *STRUCTURE TIDY*.[29] Final values of the positional and displacement parameters are given in Table 2. A full listing of interatomic distances is given in Table S1 in the Supporting Information; an abbreviated listing is provided in Table 3. Further data, in the form of crystallographic information files (CIFs), are available as Supporting Information or may be obtained from Fachinformationszentrum Karlsruhe, Abteilung PROKA, 76344 Eggenstein-Leopoldshafen, Germany (CSD Nos. 380414 and 380415).

(28) Farrugia, L. J. *J. Appl. Crystallogr.* **1999**, *32*, 837–838.
(29) Gelato, L. M.; Parthé, E. *J. Appl. Crystallogr.* **1987**, *20*, 139–143.

Table 2. Atomic Coordinates and Equivalent Isotropic Displacement Parameters for $RE_{12}Fe_{57.5}As_{41}$ (RE = La, Ce)

			$La_{12}Fe_{57.5}As_{41}$				$Ce_{12}Fe_{57.5}As_{41}$			
atom	Wyckoff position	occupancy	*x*	*y*	*z*	U_{eq} (Å^2)[a]	*x*	*y*	*z*	U_{eq} (Å^2)[a]
RE1	8g	1	0.03725(4)	0.508692(18)	0.24901(4)	0.01040(9)	0.03718(4)	0.508650(17)	0.24893(3)	0.00974(9)
RE2	8g	1	0.04672(4)	0.166281(17)	0.17206(3)	0.00960(9)	0.04781(4)	0.166359(16)	0.17310(3)	0.00861(9)
RE3	4f	1	0.53621(6)	1/4	0.67101(5)	0.00964(12)	0.53593(6)	1/4	0.67151(5)	0.00874(12)
RE4	4e	1	1/4	0.13130(2)	0.68322(5)	0.00857(12)	1/4	0.13142(2)	0.68486(5)	0.00783(11)
Fe1	8g	1	0.06436(10)	0.62211(4)	0.39906(9)	0.0099(2)	0.06429(10)	0.62231(4)	0.39807(9)	0.00820(19)
Fe2	8g	1	0.08146(11)	0.10347(4)	0.40991(9)	0.0092(2)	0.08157(10)	0.10348(4)	0.41019(9)	0.00778(19)
Fe3	8g	1	0.09154(10)	0.53815(4)	0.51674(9)	0.0094(2)	0.09098(10)	0.53799(4)	0.51645(9)	0.0080(2)
Fe4	8g	1	0.12464(10)	0.19920(4)	0.87589(9)	0.0090(2)	0.12478(10)	0.19928(4)	0.87559(9)	0.00735(19)
Fe5	8g	1	0.12511(10)	0.69529(4)	0.07815(9)	0.0096(2)	0.12474(10)	0.69560(4)	0.07840(9)	0.0080(2)
Fe6	8g	1	0.12729(10)	0.60257(4)	0.04794(9)	0.0099(2)	0.12731(10)	0.60222(4)	0.04845(9)	0.0082(2)
Fe7	8g	1	0.59715(10)	0.17715(4)	0.41628(9)	0.0093(2)	0.59615(10)	0.17728(4)	0.41615(9)	0.0082(2)
Fe8	8g	1	0.62411(10)	0.59532(4)	0.09022(9)	0.0083(2)	0.62399(10)	0.59531(4)	0.09015(9)	0.00718(19)
Fe9	8g	1	0.62865(10)	0.00207(4)	0.02799(9)	0.0081(2)	0.62813(10)	0.00190(4)	0.02742(9)	0.00701(19)
Fe10	8g	0.25	0.7209(7)	0.0715(3)	0.1498(7)	0.0155(14)[b]	0.7229(7)	0.0706(4)	0.1482(8)	0.0149(14)[b]
Fe11	4f	1	0.08230(15)	1/4	0.37987(13)	0.0094(3)	0.08217(14)	1/4	0.37992(12)	0.0078(3)
Fe12	4f	0.25	0.6964(6)	1/4	0.1057(5)	0.0130(13)[b]	0.6927(6)	1/4	0.1049(5)	0.0080(11)[b]
Fe13	4e	1	1/4	0.02955(6)	0.43554(13)	0.0097(3)	1/4	0.02939(6)	0.43561(12)	0.0082(3)
Fe14	4e	1	1/4	0.06770(6)	0.09524(13)	0.0089(3)	1/4	0.06811(5)	0.09613(12)	0.0072(3)
Fe15	4e	1	1/4	0.17662(6)	0.37461(12)	0.0088(3)	1/4	0.17679(6)	0.37451(12)	0.0077(3)
Fe16	4e	1	1/4	0.51242(6)	0.65345(13)	0.0097(3)	1/4	0.51247(6)	0.65463(12)	0.0085(3)
Fe17	4e	0.50	1/4	0.5709(2)	0.8495(5)	0.0086(12)[b]	1/4	0.5714(3)	0.8510(5)	0.0082(12)[b]
Fe18	4e	1	1/4	0.60656(6)	0.54516(12)	0.0078(3)	1/4	0.60664(5)	0.54534(12)	0.0065(3)
Fe19	4e	0.50	1/4	0.62761(18)	0.2293(3)	0.0149(9)[b]	1/4	0.62819(16)	0.2303(3)	0.0133(8)[b]
Fe20	4e	0.50	1/4	0.64367(18)	0.2360(3)	0.0147(9)[b]	1/4	0.64415(15)	0.2356(3)	0.0100(7)[b]
Fe21	4e	1	1/4	0.66871(6)	0.73495(13)	0.0107(3)	1/4	0.66865(6)	0.73642(13)	0.0088(3)
Fe22	2b	1	1/4	3/4	0.56086(18)	0.0098(4)	1/4	3/4	0.56205(18)	0.0085(4)
Fe23	2a	1	1/4	1/4	0.04362(18)	0.0095(4)	1/4	1/4	0.04548(17)	0.0074(4)
Fe24	2a	1	1/4	1/4	0.54806(18)	0.0093(4)	1/4	1/4	0.55024(17)	0.0076(4)
As1	8g	1	0.01581(7)	0.63792(3)	0.20816(6)	0.00839(15)	0.01534(7)	0.63799(3)	0.20835(6)	0.00679(14)
As2	8g	1	0.02051(7)	0.06428(3)	0.06395(6)	0.00852(15)	0.02009(7)	0.06471(3)	0.06607(6)	0.00704(14)
As3	8g	1	0.09269(7)	0.18194(3)	0.50986(6)	0.00827(15)	0.09336(7)	0.18188(3)	0.51222(6)	0.00714(14)
As4	8g	1	0.09884(7)	0.05146(3)	0.56597(6)	0.00855(15)	0.09937(7)	0.05186(3)	0.56843(6)	0.00713(14)
As5	8g	1	0.60504(7)	0.09145(3)	0.31435(6)	0.00903(15)	0.60453(7)	0.09130(3)	0.31312(6)	0.00777(14)
As6	4f	1	0.01902(10)	1/4	0.00634(9)	0.0093(2)	0.01939(10)	1/4	0.00864(9)	0.00761(19)
As7	4f	1	0.60855(10)	1/4	0.28508(9)	0.0093(2)	0.60788(10)	1/4	0.28289(9)	0.0083(2)
As8	4e	1	1/4	0.02940(4)	0.82612(9)	0.0084(2)	1/4	0.02952(4)	0.82609(9)	0.00695(19)
As9	4e	1	1/4	0.09021(4)	0.28604(9)	0.0086(2)	1/4	0.09038(4)	0.28590(9)	0.00740(19)
As10	4e	1	1/4	0.15514(4)	0.00347(9)	0.0078(2)	1/4	0.15529(4)	0.00489(9)	0.00669(19)
As11	4e	1	1/4	0.53342(4)	0.11287(9)	0.0088(2)	1/4	0.53291(4)	0.11494(9)	0.00719(19)
As12	4e	1	1/4	0.55979(4)	0.37899(9)	0.0096(2)	1/4	0.55977(4)	0.37751(9)	0.00794(19)
As13	4e	1	1/4	0.66054(5)	0.93099(9)	0.0111(2)	1/4	0.66095(4)	0.93169(9)	0.0093(2)
As14	4e	1	1/4	0.68042(4)	0.42840(9)	0.0092(2)	1/4	0.68085(4)	0.42790(9)	0.00802(19)
As15	2b	1	1/4	3/4	0.18483(12)	0.0090(3)	1/4	3/4	0.18645(12)	0.0076(3)
As16	2a	1	1/4	1/4	0.24609(12)	0.0080(3)	1/4	1/4	0.24559(12)	0.0073(3)
As17	2a	1	1/4	1/4	0.74929(12)	0.0078(3)	1/4	1/4	0.74884(12)	0.0063(3)

[a] U_{eq} is defined as one-third of the trace of the orthogonalized U_{ij} tensor. [b] U_{iso}.

XPS. Measurements were performed on a Kratos AXIS 165 spectrometer equipped with a monochromatic Al Kα X-ray source (15 kV, 14 mA) and a hybrid lens with a spot size of 700 × 400 μm^2. Samples of $RE_{12}Fe_{57.5}As_{41}$ (RE = La, Ce) were ground into fine powders and pressed onto In foil, which was attached to a Cu sample holder via C tape to ensure electrical contact. The Cu sample holder was transferred to the analysis chamber of the XPS instrument within a sealed container. The pressure inside the analysis chamber was maintained at 10^{-7}−10^{-9} Pa. The typical precision of this instrument is ±0.10 eV. The samples were sputter-cleaned with an Ar^+ ion beam (4 kV, 10 mA) to reduce the presence of surface oxides.

Survey spectra were collected with a binding energy (BE) range of 0−1100 eV, a pass energy of 160 eV, a step size of 0.7 eV, and a sweep time of 180 s. The composition was determined to be consistent with the composition obtained from the single-crystal X-ray analysis. High-resolution spectra were collected with an energy envelope of 80 eV (RE 3d peaks), 40 eV (Fe 2p peak), or 20 eV (As 3d peak), a pass energy of 20 eV, a step size of 0.05 eV, and a sweep time of 180 s. No charge correction was required because these samples are good conductors. All high-resolution spectra were calibrated against the C 1s line at 284.8 eV arising from adventitious C. Although the C 1s signal overlaps with an As Auger signal, an acceptable method for checking the calibration in a metallic system such as this is to set the Fermi edge, located from the maximum of the first derivative of the valence band spectrum, to 0 eV.[30] The spectra were analyzed by using the *CasaXPS* software package.[31] The background arising from energy loss was removed by applying a Shirley-type function, and the peaks were fitted to pseudo-Voigt (70% Gaussian and 30% Lorentzian) line profiles. Because a slight reduction of the As 3d peak was observed after Ar^+ ion sputtering, only the RE 3d and Fe 2p XPS spectra will be presented, where no such reduction occurred.

(30) Briggs, D. *Surface Analysis of Polymers by XPS and Static SIMS*; Cambridge University Press: Cambridge, U.K., 1998.

(31) Fairley, N. *CasaXPS*, version 2.3.9; Casa Software Ltd.: Teighnmouth, Devon, U.K., **2003**; www.casaxps.com.

Table 3. Ranges of Interatomic Distances (Å) in $RE_{12}Fe_{57.5}As_{41}$ (RE = La, Ce)[a]

contact	coordination number	$La_{12}Fe_{57.5}As_{41}$	$Ce_{12}Fe_{57.5}As_{41}$
RE1−As	CN8	2.948(1)−3.474(1)	2.915(1)−3.461(1)
RE2−As	CN8	2.970(1)−3.483(1)	2.943(1)−3.485(1)
RE3−As	CN8	2.948(1)−3.268(1)	2.919(1)−3.247(1)
RE4−As	CN8	3.017(1)−3.203(1)	2.989(1)−3.174(1)
Fe1−As	CN5	2.486(1)−2.593(1)	2.458(1)−2.586(1)
Fe2−As	CN4	2.378(1)−2.429(1)	2.373(1)−2.418(1)
Fe3−As	CN4	2.343(1)−2.529(1)	2.346(1)−2.531(1)
Fe4−As	CN4	2.390(1)−2.469(1)	2.390(1)−2.456(1)
Fe5−As	CN4	2.360(1)−2.502(1)	2.359(1)−2.493(1)
Fe6−As	CN4	2.352(1)−2.518(1)	2.349(1)−2.508(1)
Fe7−As	CN4	2.380(1)−2.564(1)	2.381(1)−2.563(1)
Fe8−As	CN4	2.373(1)−2.421(1)	2.374(1)−2.409(1)
Fe9−As	CN4	2.325(1)−2.398(1)	2.325(1)−2.394(1)
Fe10−As[b]	CN5	2.473(9)−2.849(8)	2.482(9)−2.830(8)
Fe11−As	CN4	2.394(2)−2.480(2)	2.389(2)−2.473(2)
Fe12−As[b]	CN4	2.421(2)−2.656(7)	2.410(2)−2.593(6)
Fe13−As	CN4	2.388(1)−2.441(2)	2.396(1)−2.435(2)
Fe14−As	CN5	2.463(2)−2.614(2)	2.434(2)−2.601(2)
Fe15−As	CN4	2.415(1)−2.487(2)	2.418(1)−2.476(2)
Fe16−As	CN5	2.419(2)−2.607(2)	2.394(2)−2.595(1)
Fe17−As[b]	CN4	2.525(6)−2.646(5)	2.508(7)−2.633(5)
Fe18−As	CN4	2.398(1)−2.407(2)	2.399(1)−2.413(2)
Fe19−As[b]	CN5	2.565(4)−2.844(5)	2.539(4)−2.810(4)
Fe20−As[b]	CN5	2.578(1)−2.812(5)	2.571(1)−2.782(4)
Fe21−As	CN5	2.468(2)−2.614(2)	2.443(2)−2.608(1)
Fe22−As	CN4	2.444(2)−2.471(2)	2.438(2)−2.472(2)
Fe23−As	CN5	2.494(1)−2.558(1)	2.480(1)−2.541(1)
Fe24−As	CN5	2.497(1)−2.524(3)	2.481(1)−2.477(3)
As1−Fe	CN9	2.390(1)−2.577(1)	2.377(1)−2.570(1)
As1−RE		3.203(1)−3.375(1)	3.173(1)−3.363(1)
As2−Fe	CN8	2.325(1)−2.531(1); 2.846(8)	2.325(1)−2.521(1); 2.830(8)
As2−RE		2.970(1)−2.992(1)	2.943(1)−2.962(1)
As3−Fe	CN8	2.380(1)−2.570(1)	2.381(1)−2.550(1)
As3−RE		3.021(1)−3.060(1)	2.993(1)−3.031(1)
As4−Fe	CN8	2.343(1)−2.581(1)	2.346(1)−2.566(1)
As4−RE		2.966(1)−3.017(1)	2.933(1)−2.989(1)
As5−Fe	CN9	2.378(1)−2.614(1)	2.373(1)−2.608(1)
As5−RE		3.103(1)−3.118(1)	3.079(1)−3.093(9)
As6−Fe	CN8	2.360(1)−2.656(7)	2.359(1)−2.593(6)
As6−RE		3.010(1) (× 2)	2.983(1) (× 2)
As7−Fe	CN9	2.394(2)−2.611(1)	2.389(2)−2.604(1)
As7−RE		3.085(1) (× 2)	3.053(1) (× 2)
As8−Fe	CN9	2.398(1)−2.634(9)	2.394(1)−2.605(7)
As8−RE		3.310(1)−3.178(1)	3.294(1)−3.151(1)
As9−Fe	CN9	2.429(1)−2.487(2)	2.418(1)−2.476(2)
As9−RE		3.283(1)−3.474(1)	3.252(1)−3.461(1)
As10−Fe	CN8	2.373(1)−2.529(2)	2.374(1)−2.508(2)
As10−RE		3.075(1) (× 2)	3.047(1) (× 2)
As11−Fe	CN8	2.349(1)−2.614(2); 2.831(5)	2.351(1)−2.601(2); 2.835(4)
As11−RE		2.947(1) (× 2)	2.915(1) (× 2)
As12−Fe	CN9	2.407(2)−2.593(1)	2.413(2)−2.586(1)
As12−RE		3.123(1) (× 2)	3.100(1) (× 2)
As13−Fe	CN9	2.421(2)−2.528(9)	2.410(2)−2.538(9)
As13−RE		3.483(1) (× 2)	3.485(1) (× 2)
As14−Fe	CN9	2.401(2)−2.592(4)	2.401(2)−2.576(4)
As14−RE		3.191(1) (× 2)	3.172(1) (× 2)
As15−Fe	CN8	2.372(1) (× 4); 2.812(5) (× 2)	2.367(1) (× 4); 2.782(4) (× 2)
As15−RE		2.948(1) (× 2)	2.919(1) (× 2)
As16−Fe	CN9	2.480(2)−2.540(3)	2.473(2)−2.495(3)
As16−RE		3.226(1) (× 4)	3.196(1) (× 4)
As17−Fe	CN9	2.469(1)−2.524(3)	2.456(1)−2.477(3)
As17−RE		3.167(1)−3.267(1)	3.143(1)−3.245(1)

[a] Distance cutoffs of 3.5 Å for RE−As and 3.0 Å for Fe−As contacts. [b] Partially occupied sites, with occupancies of 0.25 (Fe10 and Fe12) or 0.50 (Fe17, Fe18, and Fe20).

Electrical and Magnetic Properties. Needle-shaped single crystals of $Ce_{12}Fe_{57.5}As_{41}$, whose identities were confirmed by EDX analysis, were mounted for electrical resistivity measurements, made between 2 and 300 K by standard four-probe techniques on a Quantum Design Physical Property Measurement System (PPMS) equipped with an alternating-current (ac) transport controller (model 7100). The current was 100 μA, and the frequency was 16 Hz. The resistivity was measured along the needle axis of the crystals, which corresponds to the crystallographic *b* axis.

Measurements of the direct-current (dc) magnetic susceptibility were made on powders of $RE_{12}Fe_{57.5}As_{41}$ (RE = La, Ce) between 2 and 300 K under an applied field of 0.5 T on a Quantum Design 9T-PPMS dc magnetometer/ac susceptometer.

Susceptibility values were corrected for contributions from the holder and sample diamagnetism.[32]

Results and Discussion

Structure and Bonding. The ternary rare-earth iron arsenides $RE_{12}Fe_{57.5}As_{41}$ (RE = La, Ce) crystallize in a new orthorhombic structure type (space group *Pmmn*) that is quite complex (derived from 4 RE, 24 Fe, and 17 As sites). Although the structure extends in three dimensions, it is convenient to decompose it into three types of layers that stack along the shortest axis, *a*, in the sequence shown in Figure 1. Focusing on the As atoms alone, we find that they essentially lie on three sets of planes: $x = 0$, $^1/_2$ (layer A), $x = 0.1, 0.4, 0.6, 0.9$ (layer B), and $x = {}^1/_4$, $^3/_4$ (layer C). The coordination polyhedra around each As atom are then constructed by identifying the neighboring RE and Fe atoms. Each layer is made up of As-centered polyhedra that are condensed into infinite undulating chains extending along the *b* direction. To facilitate the description of these polyhedra, only one member within the two sets of split Fe sites (Fe10/Fe17 and Fe19/Fe20) is portrayed, and Fe12 atoms are considered to reside fully in higher-symmetry 2b sites instead of being partially occupied within 4f sites. With this simplification, all 17 As sites are revealed to be centered within either eight- or nine-coordinate polyhedra (Table S2 in the Supporting Information). For concreteness in the discussion below, we refer to the La compound when metrical details are provided.

Layer A consists of polyhedra centered by As1, As2, and As6 atoms. The geometry is eight-coordinate in the form of a distorted bicapped trigonal prism (As2 and As6) or nine-coordinate in the form of a monocapped tetragonal antiprism (As1). These polyhedra are connected through common vertices and edges, thereby rendering As−As contacts too long for bonding interactions. The As atoms are surrounded by Fe atoms at distances of 2.3254(14)−2.656(7) Å and by La atoms at distances of 2.9700(9)−3.3754(10) Å.

Layer B consists of polyhedra centered by As3, As4, As5, and As7 atoms. All of these As atoms reside within trigonal prisms that are either bicapped (As3 and As4) or tricapped (As5 and As7). Because the connection between these polyhedra is realized through the sharing of common faces, the As−As contacts are shorter [As7−As7, 3.0802(16) Å; As5−As5, 3.1567(11) Å; As4−As4, 3.2917(11) Å] but still nonbonding. In this layer, the shortest As−Fe distance is 2.3432(14) Å (As4−Fe3) and the shortest As−La distance is 2.9656(9) Å (As4−La1).

Layer C consists of polyhedra centered by the atoms As8−As17. Most of these As atoms have coordination environments in the form of trigonal prisms that are bicapped (As10, As11, and As15) or tricapped (As9, As12, As14, and As16). These trigonal prisms are connected together through common edges and form infinite chains of $RE_4M_{15}X_9$ fragments that are separated by REM_6X_3 blocks. Tetragonal prisms centered by As8, As13, and As17 atoms serve to bind these chains by connecting to the trigonal prisms through common edges. Such an arrangement does not allow As−As bonding.

(32) Mulay, L. N.; Boudreaux, E. A. *Theory and Applications of Molecular Diamagnetism*; Wiley: New York, 1976.

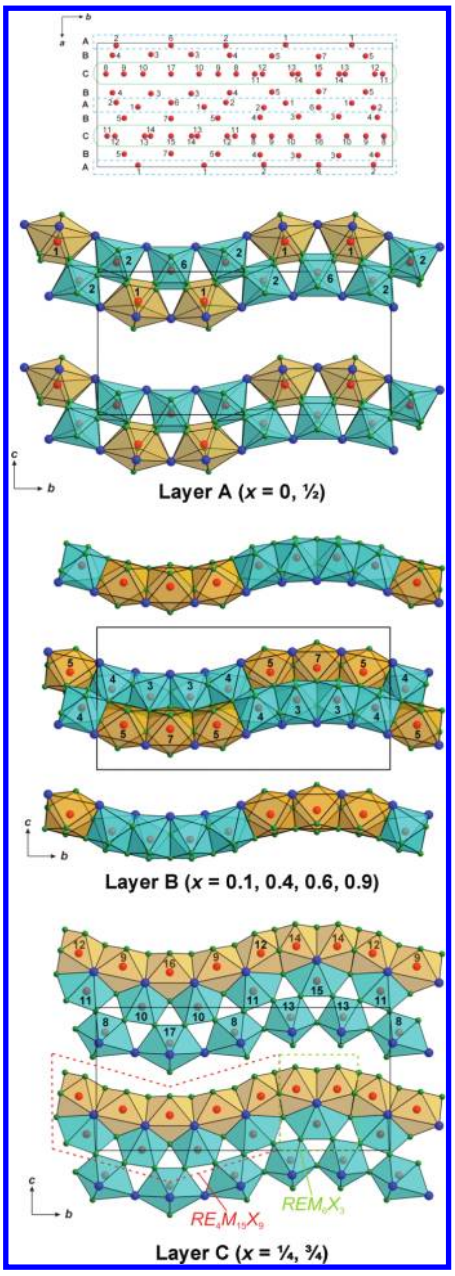

Figure 1. Structure of $RE_{12}Fe_{57.5}As_{41}$ (RE = La, Ce) in terms of a stacking of layers (A−C) along the *a* axis, with As atoms numbered. The individual layers, viewed along the *a* direction, are constructed from eight- (cyan) or nine-coordinate (orange) polyhedra centered by As atoms. The large blue spheres are RE atoms, the small green spheres are Fe atoms, and the medium red spheres are As atoms.

The shortest As−As distance observed [As12−As14, 3.1678(15) Å] is caused by strong deformation of the respective prisms, related to their stacking through a common face. In this layer, the As atoms are surrounded by Fe atoms at distances of 2.3494(15)−2.844(5) Å and by La atoms at distances of 2.9475(8)−3.4741(10) Å.

Inspection of the layer stacking sequence (Figure 1) reveals that the undulating chains in one layer fit into the grooves of the surrounding layers, through edge and face sharing of the polyhedra. These layers are held together not only by the expected heteroatomic bonding interactions (RE−As and Fe−As) but also, surprisingly, by homoatomic Fe−Fe bonding interactions, as discussed further below.

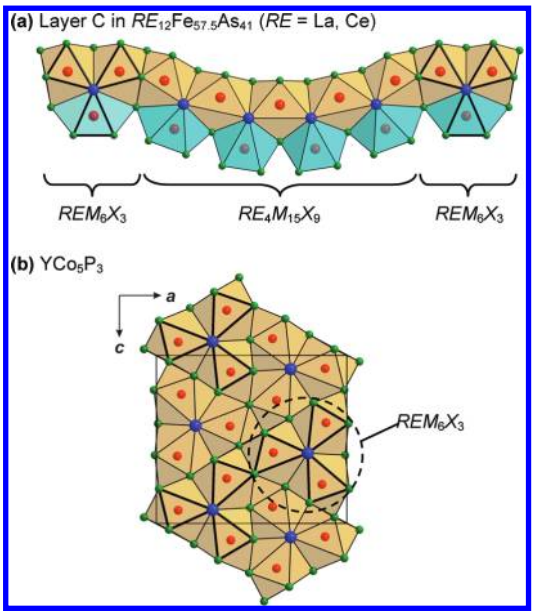

Figure 2. REM_6X_3 blocks formed by condensed trigonal prisms in (a) $RE_{12}Fe_{57.5}As_{41}$ and (b) YCo_5P_3.

The structure of $RE_{12}Fe_{57.5}As_{41}$ (RE = La, Ce) is unique, but the emphasis on As-centered polyhedra is helpful in drawing out relationships to other ternary metal-rich pnictides. For a large family of structures (usually hexagonal) where the metal-to-metalloid ratio is close to 2:1, a classifying principle has been established by noting how various trigonal prisms centered by metalloid atoms are condensed.[33−38] Although the formula $RE_{12}Fe_{57.5}As_{41}$ (RE = La, Ce) has a metal-to-metalloid ratio closer to 3:2, not 2:1, the REM_6X_3 block, which forms part of layer C in this compound, is also a basic building unit in the YCo_5P_3-type structure (Figure 2).[39] This REM_6X_3 block consists of three pnicogen-centered trigonal prisms condensed along a common edge formed by the RE atoms, forming a propeller-shaped unit. (For simplicity, the capping atoms decorating these trigonal prisms are neglected.) These REM_6X_3 blocks are connected to each other in YCo_5P_3 but are separated by intervening $RE_4M_{15}X_9$ blocks, which are also built from the principle of condensing trigonal prisms, in $RE_{12}Fe_{57.5}As_{41}$.

An alternative approach is to focus on the coordination of As atoms around the Fe atoms. In $RE_{12}Fe_{57.5}As_{41}$, most of the Fe atoms are surrounded tetrahedrally by As atoms (CN4), a coordination environment that is also frequently observed for late transition metals in ternary metal-rich pnictides with a metal-to-metalloid ratio close to 2:1.[33−38] These Fe atoms are associated with the shortest Fe−As distances, in the range of 2.325−2.656 Å,

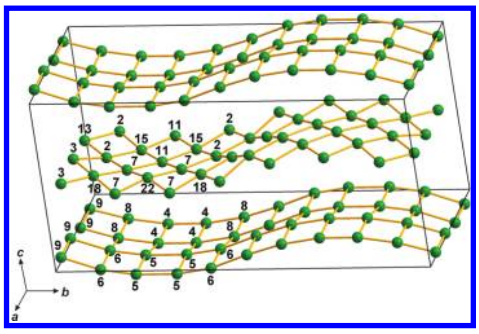

Figure 3. Fe−Fe bonding network in $RE_{12}Fe_{57.5}As_{41}$. Only distances shorter than 2.8 Å are shown. Fe atoms above and below each net are omitted.

in the structure. The remaining Fe atoms are centered within tetragonal pyramids or trigonal bipyramids, with generally longer Fe−As distances, in the range of 2.419−2.849 Å, because of the higher coordination number (CN5).

The Zintl−Klemm concept serves as a reasonable starting point for the development of the electronic structure. The absence of As−As bonding, highlighted in the preceding structural analysis in terms of As-centered polyhedra, implies an assignment of isolated As^{3-} species. With the assumption of full electron transfer from the La atoms, the requirement for charge balance leads to the formulation $(La^{3+})_{12}(Fe^{1.5+})_{57.5}(As^{3-})_{41}$. The low oxidation state deduced for the Fe atoms suggests the possibility for additional metal−metal bonding interactions to take place. The La−As (> 2.947 Å) and Fe−As distances (> 2.325 Å) in $La_{12}Fe_{57.5}As_{41}$ are similar to those in $LaFe_4As_{12}$ (3.152 and 2.365 Å, respectively).[9] There are numerous Fe−Fe interactions in $La_{12}Fe_{57.5}As_{41}$, mostly ranging from 2.5 to 2.7 Å, which are similar to those found in Fe_2As and $Fe_{12}As_5$,[40,41] where metal−metal bonding is implicated. However, there are a few even shorter ones, down to 2.418 Å (Fe5−Fe6), which is comparable to the 2.410 Å distance found in Fe_3P.[42] This Fe−Fe bonding network is manifested as two types of undulating square nets (if distances shorter than an arbitrary cutoff of 2.8 Å are considered) lying parallel to the *ab* plane (Figure 3), reminiscent of the flat square nets found in LaFeAsO.[3−5]

Fe 2p and RE 3d XPS Spectra. In lieu of an electronic band structure calculation (which was attempted with the linear muffin-tin orbital (LMTO) method but was intractable because of the sheer size of the problem, with over 200 atoms in the unit cell!), core-line XPS spectra were measured for $RE_{12}Fe_{57.5}As_{41}$ (RE = La, Ce). The Fe 2p XPS spectra reveal two peaks corresponding to the $2p_{3/2}$ and $2p_{1/2}$ spin−orbit-coupled final states (Figure 4). The single set of Fe 2p signals implies that no distinction can be made for the different Fe sites (CN4 and CN5) present in the crystal structure. Moreover, the Fe $2p_{3/2}$ BE of 707.0 eV (for both RE members) is essentially identical with that in the Fe metal (706.9 eV),[43] in

(33) Pivan, J.-Y.; Guérin, R.; Sergent, M. *J. Solid State Chem.* **1987**, *68*, 11–21.
(34) Pivan, J.-Y.; Guérin, R. *J. Solid State Chem.* **1998**, *135*, 218–227.
(35) Albering, J. H.; Jeitschko, W. *J. Alloys Compd.* **1996**, *241*, 44–50.
(36) Jeitschko, W.; Terbüchte, L. J.; Rodewald, U. Ch. *Z. Anorg. Allg. Chem.* **2001**, *627*, 2095–2099.
(37) Jeitschko, W.; Terbüchte, L. J.; Rodewald, U. Ch. *Z. Anorg. Allg. Chem.* **2001**, *627*, 2673–2679.
(38) Babizhetskyy, V.; Le Sénéchal, C.; Guérin, R.; Isnard, O.; Hiebl, K. *Phys. Rev. B* **2002**, *66*, 014102-1–014102-11.
(39) Jeitschko, W.; Meisen, U.; Scholz, U. D. *J. Solid State Chem.* **1984**, *55*, 331–336.
(40) Nuss, J.; Wedig, U.; Jansen, M. *Z. Kristallogr.* **2006**, *221*, 554–562.
(41) Maaref, S.; Madar, R.; Chaudouet, P.; Fruchart, R.; Sénateur, J. P.; Averbuch-Pouchot, M. T.; Bacmann, M.; Durif, A.; Wolfers, P. *Mater. Res. Bull.* **1983**, *18*, 473–480.
(42) Rundqvist, S. *Acta Chem. Scand.* **1962**, *16*, 1–19.
(43) Grosvenor, A. P.; Wik, S. D.; Cavell, R. G.; Mar, A. *Inorg. Chem.* **2005**, *44*, 8988–8998.

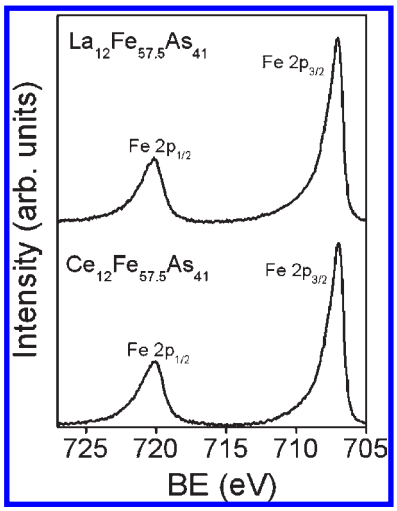

Figure 4. Fe 2p XPS spectra for $La_{12}Fe_{57.5}As_{41}$ and $Ce_{12}Fe_{57.5}As_{41}$.

apparent contradiction to an expected shift to higher BE if the presence of positively charged Fe species, predicted from the Zintl−Klemm analysis above, is taken at face value. However, the Fe $2p_{3/2}$ BE frequently does not experience significant shifts relative to Fe metal even when there should be nominal differences in the Fe oxidation state, as seen in the series FeP (706.9 eV), Fe_2P (706.8 eV), and Fe_3P (706.9 eV).[43,44] Importantly, the peaks exhibit asymmetric line shapes that can be traced to the electronic delocalization characteristic of metallic solids, including Fe metal itself.[45] (The asymmetry arises when valence electrons, interacting with the core hole remaining after the photoelectron is ejected, are scattered into the continuum of empty conduction states near the Fermi edge.) The lack of a shift in the $2p_{3/2}$ BE is thus not necessarily indicative of a zerovalent state but rather because the core electrons experience greater nuclear screening as a result of the electronic delocalization likely related to metal−metal bonding interactions. A similar interpretation has been proposed for LaFeAsO, which also shows little shift in the Fe $2p_{3/2}$ BE (707.1 eV) but exhibits metal−metal interactions at even longer Fe−Fe separations of 2.8 Å.[46]

The RE 3d XPS spectra consist of two main peaks representing the $3d_{5/2}$ (A) and $3d_{3/2}$ (B) spin−orbit-coupled final states (Figure 5). The La $3d_{5/2}$ BE is 834.9 eV and the Ce $3d_{5/2}$ BE is 882.1 eV, but it is difficult to interpret BE shifts for RE atoms because of their greater sensitivity to the coordination environment and final state effects.[47] (Ce 3d BEs may also be potentially influenced by the effects of poor screening by 4f electrons.[48]) However, the line shapes of these peaks do reveal information about the valence state of the RE atoms. The similarity of the line shapes in these spectra to those of various reference compounds (LaP, CeF_3, $LaFe_4P_{12}$, and

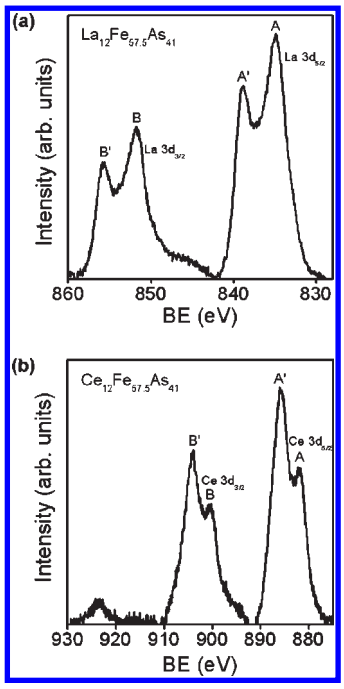

Figure 5. RE 3d XPS spectra for (a) $La_{12}Fe_{57.5}As_{41}$ and (b) $Ce_{12}Fe_{57.5}As_{41}$, with the main core lines (A and B) and satellite peaks (A′ and B′) identified.

$CeFe_4P_{12}$)[47] confirms the presence of trivalent La^{3+} and Ce^{3+} species in $RE_{12}Fe_{57.5}As_{41}$ (RE = La, Ce). Satellite peaks (A′ and B′) are seen at higher BE to the main core-line peaks. It is generally believed that a ligand-to-metal charge-transfer shakeup process is responsible for these satellite peaks, whose relative intensities depend on the overlap between metal and ligand orbitals.[49,50] The additional overlap provided by virtue of a greater f-electron density in the Ce atoms leads to the more intense satellite peaks in $Ce_{12}Fe_{57.5}As_{41}$. An alternative mechanism has been proposed in which the satellite is attributed to a shakeup process of RE valence electrons into empty conduction states,[51] but this can be ruled out for $La_{12}Fe_{57.5}As_{41}$ because there are no filled La-based valence states available.

Properties. Magnetic measurements have been made on powder samples of $RE_{12}Fe_{57.5}As_{41}$ (RE = La, Ce) (Figure 6). The zero-field-cooled dc magnetic susceptibility curves show rapid increases, indicative of ferromagnetic behavior, below Curie temperatures, T_C, of 125 K (RE = La) or 95 K (RE = Ce) [as located from plots of $d(\chi T)/dT$ vs T (not shown)]. The isothermal magnetization curves at 2 K reveal an approach to saturation at high applied fields, up to about 40 μ_B/fu for both compounds. Above T_C, interestingly, the inverse magnetic susceptibility curves are distinctly nonlinear (insets in Figure 6a,c) so that a Curie−Weiss fitting cannot be applied. Indeed, even at 300 K, the magnetization curves still exhibit saturation behavior but to a lower value, about 5 μ_B/fu. Although it is tempting to suggest the occurrence of another ferromagnetic transition with a T_C higher than 300 K, we cannot rule out the possibility that these observations could be

(44) Blanchard, P. E. R.; Grosvenor, A. P.; Cavell, R. G.; Mar, A. *Chem. Mater.* **2008**, *20*, 7081–7088.
(45) Doniach, S.; Šunjić, M. *J. Phys. C: Solid State Phys.* **1970**, *3*, 285–291.
(46) Blanchard, P. E. R.; Slater, B. R.; Cavell, R. G.; Mar, A.; Grosvenor, A. P. *Solid State Sci.* **2009**, *12*, 50–58.
(47) Grünert, W.; Sauerlandt, U.; Schlögl, R.; Karge, H. G. *J. Phys. Chem.* **1993**, *97*, 1413–1419.
(48) Grosvenor, A. P.; Cavell, R. G.; Mar, A. *Chem. Mater.* **2006**, *18*, 1650–1657.
(49) Ikeda, T.; Okada, K.; Ogasawara, H.; Kotani, A. *J. Phys. Soc. Jpn.* **1990**, *59*, 622–630.
(50) Niu, C. J.; Jia, Y. Q. *Spectrochim. Acta, Part A* **1993**, *49*, 947–951.
(51) Imada, S.; Jo, T. *J. Phys. Soc. Jpn.* **1989**, *58*, 402–405.

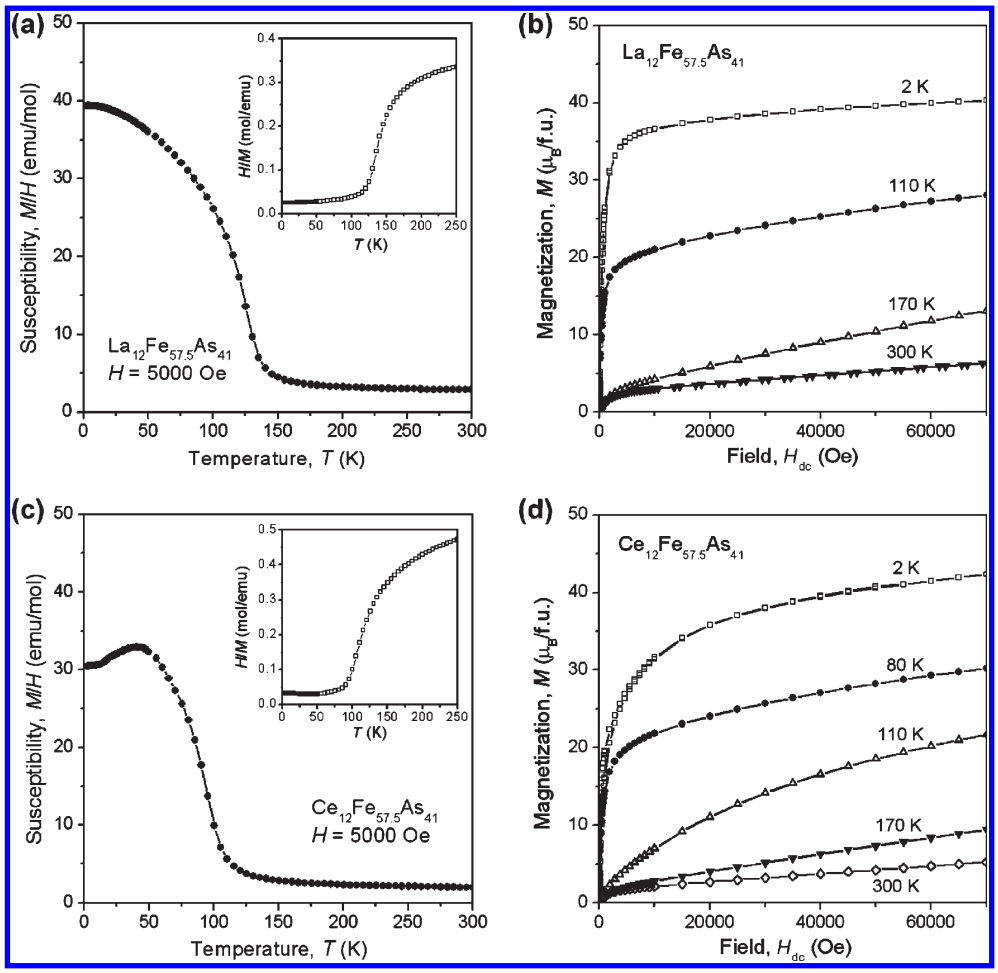

Figure 6. Magnetic data for (a and b) $La_{12}Fe_{57.5}As_{41}$ and (c and d) $Ce_{12}Fe_{57.5}As_{41}$. The left panels show the zero-field-cooled dc magnetic susceptibility (insets: inverse magnetic susceptibility) as a function of the temperature, and the right panels show isothermal magnetization curves at various temperatures.

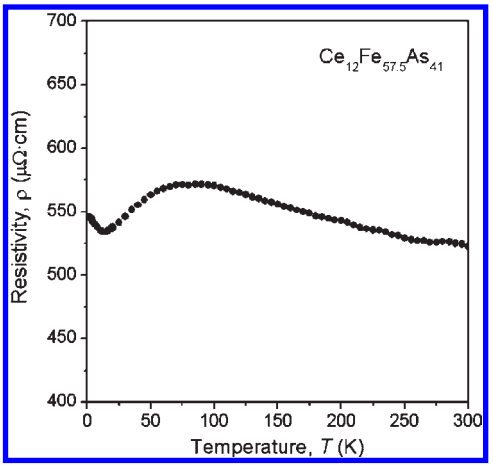

Figure 7. Electrical resistivity of $Ce_{12}Fe_{57.5}As_{41}$.

caused by small amounts of ferromagnetic impurities (such as Fe or perhaps other binary phases), especially considering the large loading fraction of Fe used in the synthesis of these compounds. Within the detection limit of powder X-ray diffraction analysis, no impurity phases were found in the samples used for magnetic measurements. However, trace Fe inclusions have been identified to be a problem, for example, plaguing the synthesis of $LaFe_{13-x}Si_x$ phases even after extended annealing.[52] Further measurements, at temperatures higher than 300 K or on single crystals, may help resolve some of these ambiguities.

The electrical resistivity for $Ce_{12}Fe_{57.5}As_{41}$ gradually increases to a maximum at 85 K (close to the T_C of 95 K observed in the magnetic susceptibility) and falls to a minimum at 10 K before rising again slightly as the temperature is lowered (Figure 7). The absolute values for the resistivities themselves are quite high. The resistivity profile is characteristic of other cerium intermetallics exhibiting Kondo lattice effects.[53] In combination with the magnetic results, the picture that emerges is that there is strong electron correlation, involving the interaction of conduction electrons with localized magnetic moments.

The discovery of the new phases $RE_{12}Fe_{57.5}As_{41}$ (RE = La, Ce) through a systematic investigation of the RE−Fe−As systems provides impetus for further study of the ternary rare-earth arsenides. The structural theme of pnicogen-centered trigonal prisms continues to be a robust one that is exhibited by many metal-rich pnictides,

(52) Liu, T.; Chen, Y.; Tang, Y.; Xiao, S.; Zhang, E.; Wang, J. *J. Alloys Compd.* **2009**, *475*, 672–675.

(53) Thomas, E. L.; Millican, J. N.; Okudzeto, E. K.; Chan, J. Y. *Comments Inorg. Chem.* **2006**, *27*, 1–39.

with additional diversity being introduced here by the condensation of these trigonal prisms in new ways. XPS measurements generally support the presence of trivalent RE species as well as considerable electronic delocalization experienced by the Fe metal centers, which are arranged in unusual undulating square nets.

Acknowledgment. The Natural Sciences and Engineering Research Council of Canada and the University of Alberta supported this work. We thank Dr. Robert McDonald and Dr. Michael J. Ferguson (X-ray Crystallography Laboratory) for the X-ray data collection and Christina Barker (Department of Chemical and Materials Engineering) for assistance with the EDX analysis.

Supporting Information Available: X-ray crystallographic files in CIF format and additional tables of crystallographic data. This material is available free of charge via the Internet at http://pubs.acs.org.